



# Persistent slip observed in TiZrNbHfTa: A body-centered high-entropy cubic alloy

Masaki Tanaka<sup>a,b,\*</sup>, Shinji Okajo<sup>c</sup>, Shigeto Yamasaki<sup>a</sup>, Tatsuya Morikawa<sup>a</sup>

<sup>a</sup> Department of Materials, Kyushu University, 744 Motooka, Nishi-ku, Fukuoka 819-0395, Japan

<sup>b</sup> Center for Elements Strategy Initiative for Structural Materials, Kyoto University, Sakyo-ku, Kyoto 606-8501, Japan

<sup>c</sup> Graduate School of Engineering, Kyushu University, 744 Motooka, Nishi-ku, Fukuoka 819-0395, Japan

## ARTICLE INFO

### Article history:

Received 7 January 2021

Revised 19 March 2021

Accepted 20 March 2021

Available online 8 April 2021

### Keywords:

HEA

Cross-slip

Refractory alloy

Deformation

Critical resolved shear stress

## ABSTRACT

Slip properties of TiZrNbHfTa were evaluated to obtain  $\psi$ - $\chi$  relationships, where  $\chi$  is defined as the angle between the maximum shear stress plane and  $(\bar{1}01)$ .  $\psi$  is defined as the angle between the apparent slip plane and  $(\bar{1}01)$ . Bending tests were conducted with micrometer-sized cantilevers fabricated from a single grain with a focused ion beam. Slip bands appear to be straight on a micrometer length-scale, as for Fe-Si alloys, which suggests a persistent slip. However, the  $\psi$ - $\chi$  relationship indicated that  $\psi$  is nearly the same as  $\chi$ , suggesting that there is no persistent slip. Detailed observations with an atomic force microscope confirm that cross-slipping is so frequent at a sub-micrometer length-scale that the slip bands appear to be straight and the maximum shear stress plane is observed on a micrometer length-scale. Here, TiZrNbHfTa shows abnormally frequent cross-slipping, which is a novel characteristic of high-entropy body-centered cubic alloys.

© 2021 The Authors. Published by Elsevier Ltd on behalf of Acta Materialia Inc.

This is an open access article under the CC BY license (<http://creativecommons.org/licenses/by/4.0/>)

Slip bands are formed on a specimen surface when dislocations are left off at the surface during slip deformations. Slip bands in body-centered cubic (BCC) metals are often reported to be wavy, described as a “pencil glide”. Dislocations in BCC metals frequently cross-slip, changing slip planes between the  $\{110\}$  and  $\{112\}$  planes during plastic deformation. Thus, the apparent slip plane is not specified as the  $\{110\}$  or  $\{112\}$  plane, on which the Burgers vector is. In Nb-Mo alloys, the apparent slip plane at room temperature is the plane for which the resolved shear stress is at a maximum [1–5], which is called the maximum shear stress plane (MSSP). The frequency of cross-slipping, in other words, the magnitude of the pencil glide, is influenced by the contents of the solid solutes. For example, pencil gliding is suppressed by silicon in steel, that is, cross-slipping is suppressed in Fe-Si alloys. Slip bands lie exactly on the same  $\{110\}$  plane when the crystal deforms and show persistent slipping with straight slip bands. It has been reported that this tendency is enhanced in the presence of a greater amount of solid solute Si [2–4].

BCC high-entropy alloys have drawn attention as refractory alloys because they maintain high strength even at high temperatures [6–20]. However, there remain some questions regarding the

mechanical properties of BCC high-entropy alloys [16–18,21–24]. For example, it has been reported that slip bands in BCC high-entropy alloys tend to be straight. Fig. 1 shows a scanning electron microscope (SEM) image of TiZrNbHfTa, a BCC high-entropy alloy, after rupture in a tensile test at room temperature. The right end of the figure shows the fractured area of the parallel portion. There are many slip bands in each grain on the specimen surface and the slip bands are straight, indicating suppression of cross-slipping, which is common for Fe-Si alloys. Thus, the slip planes could be either  $\{110\}$  or  $\{112\}$  planes in this alloy system as well as other Fe-Si alloys. In this study, therefore, the magnitude of the persistent slip of a BCC high-entropy alloy of TiZrNbHfTa will be examined by measuring the  $\psi$ - $\chi$  relationship. Traditionally, single crystals are used to reveal the  $\psi$ - $\chi$  relationship, however this approach requires the use of a single crystal of sufficient size for tensile testing. Rather than using a large single crystal, we used micrometer-sized cantilevers fabricated from a sufficiently large grain to perform bending tests to measure the  $\psi$ - $\chi$  relationship.

We used a BCC high-entropy alloy of an isoatomic ratio, TiZrNbHfTa. An ingot was obtained by arc melting [13]. The average grain size was approximately 230  $\mu\text{m}$  in an equivalent diameter. The carbon impurity concentration was 0.002 mass%. Electron backscatter diffraction observations indicated equiaxial grains without dendrite formation. Micrometer-sized cantilevers

\* Corresponding author.

E-mail address: [masaki@zaiko.kyushu-u.ac.jp](mailto:masaki@zaiko.kyushu-u.ac.jp) (M. Tanaka).

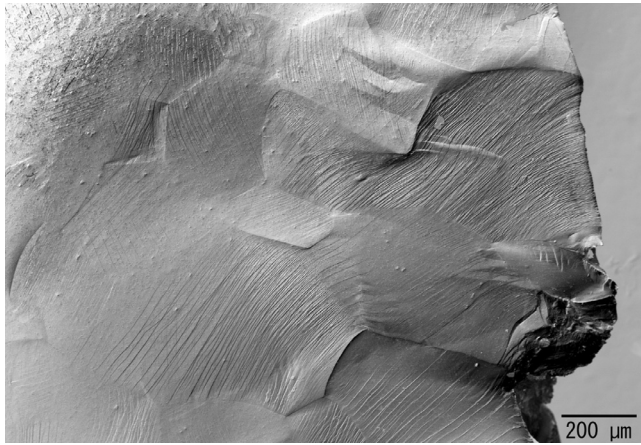


**Fig. 1.** SEM image of a specimen surface after a tensile test in TiZrNbHfTa at room temperature. Straight slip bands are seen in each grain.

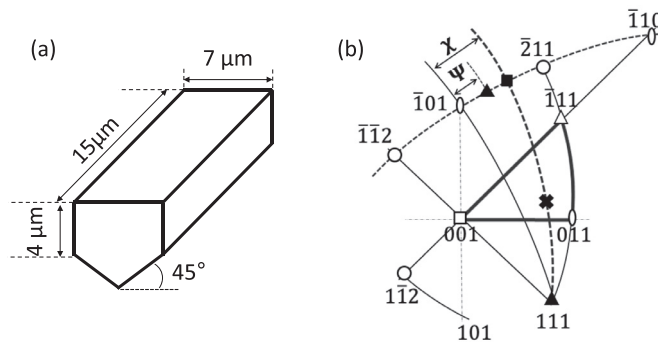


**Fig. 2.** (a) Schematic drawing of micro-sized cantilever fabricated in this study with a focused ion beam. (b) Definition of  $\psi$  and  $\chi$  on a [001] stereograph. Tensile direction is denoted as ✱ in the standard triangle. Directions of maximum shear stress plane and apparent slip plane are denoted as ■ and ▲, respectively.

were fabricated from a grain with a focused ion beam (FEI, Helios Nanolab 600i), as shown in Fig. 2(a). The length, width, and thickness of the cantilevers were 15, 7, and 10  $\mu\text{m}$ , respectively. A flat-punch-type indent was pushed down at the near edge of the cantilever in the bending tests at room temperature, whereas tensile stress was applied to the top surface of the cantilever, with a nano indentation tester (ELIONIX, ENT-1100b). The indent moved 1.5  $\mu\text{m}$  after making contact with the cantilever at a rate of 15 nm/sec. A total of 23 specimens with different crystallographic directions in the length direction of the cantilever were used in the bending tests. Slip bands formed after the bending tests were observed with a scanning electron microscope (Hitachi, SU5000) and an atomic force microscope (Shimazu, SPM-9700HT).

In this study, the  $\psi$ - $\chi$  relation was determined to evaluate the magnitude of cross-slipping by tracing slip bands on the cantilever after the bending tests. Here, the meaning of the  $\psi$ - $\chi$  relation is briefly discussed. Fig. 1(b) shows part of a [001] standard stereograph. Supposing the tensile direction, that is, the length direction of the cantilever, is set in the direction marked ✱ in the standard triangle, the slip direction becomes the [111] direction. Candidates for the slip plane must lie in the circle connecting the  $[\bar{1}\bar{1}2]$  and  $[\bar{2}11]$  directions. The MSSP, indicated as ■ in Fig. 1(b), is obtained at the junction between two great circles; one is the great circle connecting the  $[\bar{1}\bar{1}2]$  and  $[\bar{2}11]$  directions, and the other is the great circle connecting the tensile direction, marked as ✱, and the [111] direction. Here, the angle between MSSP and  $(\bar{1}01)$  is de-

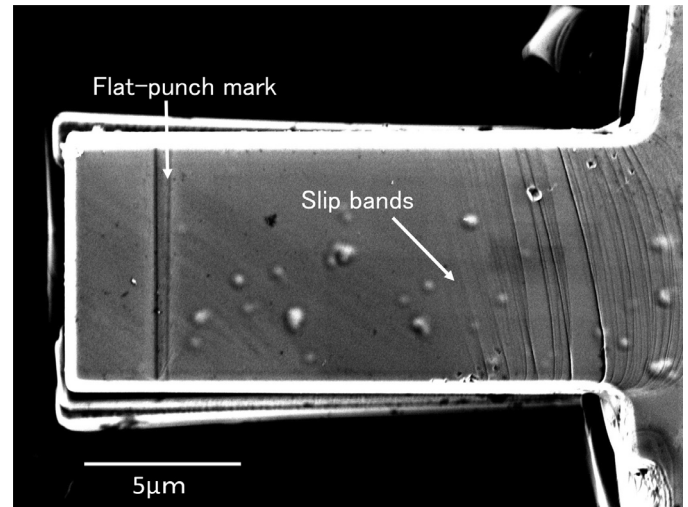


**Fig. 3.** SEM image of a cantilever after a bending test where  $\chi = 6.6^\circ$ .

fined as  $\chi$ , while the angle between the apparent slip plane and  $(\bar{1}01)$  is defined as  $\psi$ . The signs of  $\psi$  and  $\chi$  are defined as positive when the MSSP and the apparent slip planes are between  $(\bar{1}01)$  and  $(\bar{2}11)$  and as negative when they are between  $(\bar{1}01)$  and  $(\bar{1}\bar{1}2)$ . In the case of a normal pure bcc metal or dilute solid solution metal,  $\psi = \chi$  indicates that the MSSP and apparent slip planes are identical; hence, the slip planes are not persistent and frequently cross-slip.  $\psi \neq \chi$  indicates that slip planes persist with suppressed cross-slipping. The greater the divergence of  $\psi$  from  $\chi$ , the greater the persistence of the slip planes. The apparent slip planes were determined by tracing the slip bands formed on the specimen surface after bending tests.

Fig. 3 shows a SEM image of a cantilever after bending tests where the plane normal direction was (920) and the tensile direction was  $[\bar{1}59]$  where  $\chi = 6.6^\circ$ . The vertical mark on the left side is a scratch made by the flat-punch indent when the indent contacted the cantilever. Circular dots on the surface are contamination. Curved slip bands formed at the right side of the cantilever because the state of stress at the root of the cantilever is not a simple tensile condition; hence, the slip bands formed at the root are not suitable for determining the apparent slip planes. Therefore, slip trace analysis was performed at the slip bands formed furthest from the root where the state of stress can be regarded to be a simple tensile stress at the surface. Notably, the slip bands were straight, as shown in Fig. 1. The apparent slip plane was determined to be the  $(\bar{1}\bar{6}214)$  plane where  $\psi = 5^\circ$ . The  $\psi$ - $\chi$  relation was determined by repeating the bending tests of specimens in different length directions.

Fig. 4 shows a  $\psi$ - $\chi$  relation, where the dashed line in the figure denotes the line of  $\psi = \chi$ , indicating that plots from TiZrNbHfTa lie on the line. Hence, the MSSP and apparent slip plane are identical in this system at room temperature regardless of the value of  $\chi$ . This result also suggests that persistent slip does not occur. Results for Fe-4.4mass%Si alloys [4] are also plotted for reference, where most plots have  $\psi \approx 0$  where  $-15^\circ \leq \chi \leq 25^\circ$ . Thus, slips occur at the  $(\bar{1}01)$  planes. This is because cross-slipping is suppressed in Fe-Si alloys [4]. Furthermore, Fe-Si alloys have straight slip bands accompanied by a persistent slip on the  $(\bar{1}01)$  plane. That is, a persistent slip induces  $\psi \neq \chi$  in Fe-Si alloys. However, in TiZrNbHfTa, although the slip bands are straight and have persistent slips, similar to those in Fe-Si alloys, Fig. 4 indicates that  $\psi = \chi$ . This result disagrees with those from Fe-Si alloys. Specifically, the straight slip bands seen in TiZrNbHfTa are not caused by a persistent slip nor by suppression of cross-

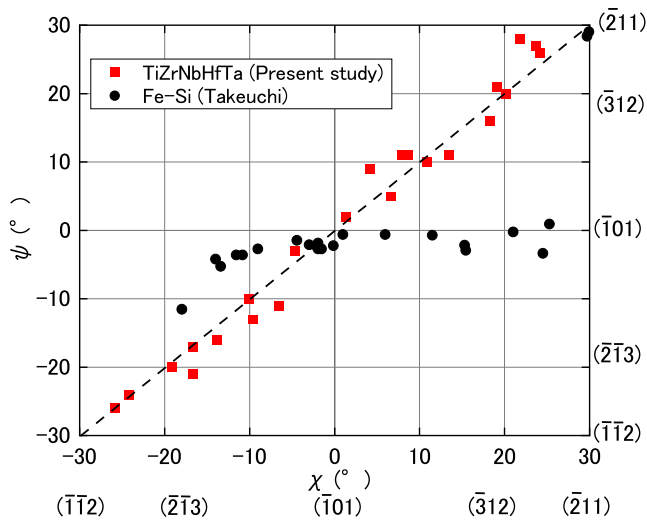


Fig. 4.  $\psi$ - $\chi$  relations from TiZrNbHfTa obtained in this study and Fe-4.4mass%Si obtained by Takeuchi et al. [4].

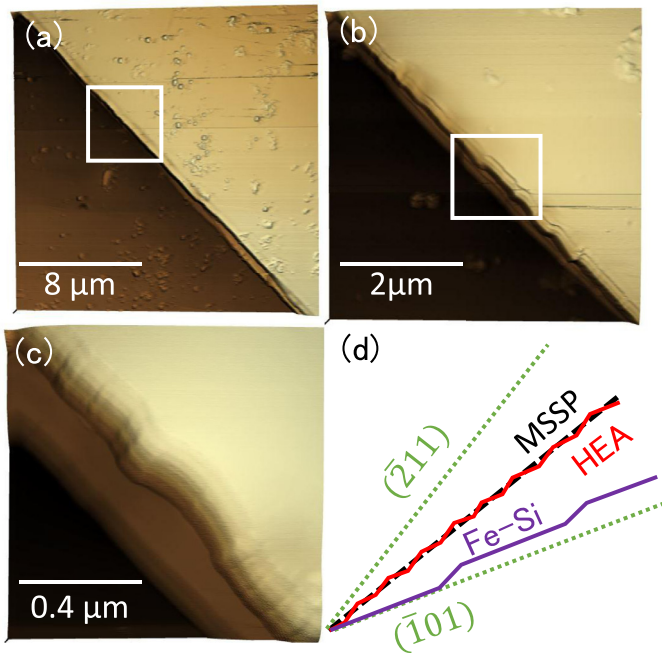


Fig. 5. (a)–(c) AFM images of slip bands in case of  $\chi = -8^\circ$ ; (b) and (c) are enlarged images of the white squares in (a) and (b), respectively. (d) Schematic of slip bands of TiZrNbHfTa (denoted as HEA), and Fe-Si.

slipping. Rather, the fact that  $\psi \approx \chi$  in TiZrNbHfTa suggests that cross-slipping in TiZrNbHfTa is so frequent that the slip bands appear to be straight, even on a micrometer length-scale. Therefore, we used atomic force microscopy (AFM) to observe the slip bands.

Fig. 5(a)–(c) show AFM images of slip bands formed on the specimen surface after the bending test with a condition of  $\chi = -8$ . The apparent slip plane was  $(\bar{2}1\ 2\ 19)$ . Fig. 5(a) shows a wide AFM image with a similar length-scale to that of the SEM images in Fig. 1, where the slip bands are also straight. However, high magnification images in Fig. 5(b) and (c) indicate that the slip bands are wavy with an interval of approximately 0.4  $\mu\text{m}$ . These observations support the assumption that cross-slippage occurs more frequently in TiZrNbHfTa than in Fe-Si alloys. Fig. 5(d) shows

a schematic of the relationship between the MSSP, slip planes of  $(\bar{1}01)$  and  $(\bar{2}11)$ , and the apparent slip traces of TiZrNbHfTa (indicated as HEA) and Fe-Si alloys. Slip bands of Fe-Si alloys, denoted by purple lines in the figure, persist on the  $(\bar{1}01)$  plane and rarely cross-slip to the  $(\bar{2}11)$  plane, resulting in the case of apparent slip bands that are straight and close to the trace made by the  $(\bar{1}01)$  plane. Conversely, the slip bands in TiZrNbHfTa, denoted by red lines in the figure, cross-slip with great frequency, which leads to the case of an apparent slip plane is close to the trace of the MSSP. Because the interval of cross-slipping in TiZrNbHfTa is of a sub-micrometer order, the slip bands appear to be straight when they are observed at a large length-scale.

Although further investigations are necessary to elucidate the reason why TiZrNbHfTa shows such frequent cross-slipping, one possibility is the random atomic arrangement of high-entropy alloys. It has been reported that this atomic arrangement in high-entropy alloys influences the possibility of cross-slipping in face centered cubic (FCC) high-entropy alloys [25–27]. Because the interaction energy depends on the pair of bonding atoms, the total energy in a local area varies from atom to atom in the crystal and is accompanied by a change in the stacking fault energy. When a dissociated screw dislocation cross-slips to another slip plane, it is necessary for the screw dislocation to partially re-combine. The large fluctuation of the energy barrier for cross-slipping, owing to the randomness of the atomic configuration in high-entropy alloys, means that there is an area having a low energy barrier close to zero along the dislocation line. The screw dislocations re-combine at some points and cross-slip to another slip plane at the point with the low energy barrier. The cross-slip mechanism in FCC crystals cannot directly apply to that of BCC crystals because the stacking fault energy in BCC crystals is so high that screw dislocations in BCC crystals are not dissociated in the same way as those in FCC crystals. However, the randomness of the atomic arrangement in BCC high-entropy alloys should also influence cross-slipping in BCC crystals.

It has been reported that Fe-Si alloys have persistent slips [2,4] and a greater Si content tends to lead to persistent slips. In those alloys, slip bands are very sharp and  $\psi \approx 0$  over a large range of  $\chi$  values. Cross-slipping is suppressed as the Si content increases, that is, slip bands become sharper, and the  $\psi$ - $\chi$  relationship becomes  $\psi \neq \chi$ . Notably, this tendency of the  $\psi$ - $\chi$  relationship is unlike that of TiZrNbHfTa, where  $\psi \approx \chi$ , even though both alloys have sharp slip bands. Although the mechanism behind the persistent slip in Fe-Si alloys has not been clarified yet, one proposed mechanism invokes a process of double-kink nucleation [28]. Molecular dynamics simulation has shown that screw dislocations and Si atoms have an attractive interaction; hence, there is an increased chance of kink formation as the content of Si increases. Mohri et al. [28] suggested that many kink-pairs are formed on different  $\{110\}$  planes along a screw dislocation and the kink-pairs migrate along the dislocation line. When two kink-pairs meet each other along the screw dislocation, jogs are formed, which suppress cross-slipping.

If the randomness of the atomic arrangement in TiZrNbHfTa enhances only kink-pair formation, cross-slipping should be suppressed, as suggested in Fe-Si alloys; however, this behavior disagrees with the experimental results of  $\psi \approx \chi$  obtained in this study. It is known that the migration energy for kink-pairs is much smaller than that for kink-pair nucleation, then the time for kink-pair migration is negligible in the process of dislocation motion. It is presumed that if the length of the edge-segment of kink-pairs in TiZrNbHfTa is only one atomic distance or close to that length-scale, the screw dislocation should easily cross-slip to other  $\{110\}$  planes once a kink-pair is nucleated at one point along the dislocation segment. This mechanism explains the experimental results of both  $\psi \approx \chi$  and persistent slips.



Another possible mechanism could involve a change in the core structure of screw dislocations. Yin et al. [29] used density functional theory calculations to estimate the core energy of a screw dislocation in a BCC high-entropy alloy of MoNbTaW. They suggested that the Peierls barrier of screw dislocations depends on the types of atoms adjacent to the dislocation core. This is because the magnitude of each type of atomic bonding is different among the different atoms unlike the uniform bonding in a pure or a dilute solid solution metal. In the case of the MoNbTaW system, the Peierls barrier for Nb is lowest and that of W is highest. This suggests that cross-slipping is enhanced when a screw dislocation moves at the atoms with weak bonding, which is consistent with the frequent cross-slipping in TiZrNbHfTa, as shown in Fig. 5. Although there have been no direct calculations to date for the TiZrNbHfTa alloy system, a similar mechanism would mediate the frequent cross-slipping found in this study. A double kink should form in the direction where the Peierls potential is relatively low. Rao et al. [30] used molecular dynamics and first-principal calculations to examine dislocation core structures of  $a/2\langle 111 \rangle$  screw dislocations in NbTiZr tertiary alloys. They showed that the dislocation core spreads on different  $\{110\}$  planes along the dislocation and both the magnitude and spreading of the  $\{110\}$  planes depend on the position along the dislocation line. This behavior reflects the three-dimensional randomness of the atomic arrangement near the dislocation core.

In conclusion, a  $\psi$ - $\chi$  relation obtained by micro-cantilever bending tests suggests that there is no persistent slip in TiZrNbHfTa, although the slip bands are straight. Cross-slipping in this alloy is so frequent that apparent slip bands take on the appearance of the MSSP. The  $\psi$ - $\chi$  relation also depends on temperature; hence, the temperature dependence of cross-slipping is another aspect of interest for understanding the mechanical properties of high-entropy BCC alloys. We note here that interstitial atoms should influence the  $\psi$ - $\chi$  relation not only in high-entropy alloys but also in other bcc atoms, which will be reported in our future work.

#### Declaration of Competing Interest

The authors declare that they have no known competing financial interests or personal relationships that could have appeared to influence the work reported in this paper.

#### Acknowledgements

The authors appreciate that this work is partly supported by JSPS KAKENHI Grant-in-Aid for Scientific Research on Innovative Areas (JP18H05451) and Element Strategy Initiative of MEXT, Grant Number JPMXP0112101000.

#### References

- [1] C.D. Statham, D. Vesely, J.W. Christian, *Acta Metall* 18 (1970) 1243–1251.
- [2] T. Taoka, S. Takeuchi, E. Furubayashi, *J. Phys. Soc. Jpn.* 19 (1964) 701–711.
- [3] B. Šesták, N. Zarubova, *Phys. Stat. Sol. (b)* 10 (1965) 239–250.
- [4] S. Takeuchi, E. Furubayashi, T. Taoka, *Acta Metall.* 15 (1967) 1179–1191.
- [5] W.A. Spitzig, A.S. Keh, *Metallurgical Transactions* 1 (1970) 2751–8.
- [6] Y.F. Ye, Q. Wang, J. Lu, C.T. Liu, Y. Yang, *Materials Today* 19 (2016) 349–362.
- [7] H.Y. Diao, R. Feng, K.A. Dahmen, P.K. Liaw, *Current Opinion in Solid State and Materials Science* 21 (2017) 252–266.
- [8] D.B. Miracle, M.-H. Tsai, O.N. Senkov, V. Soni, R. Banerjee, *Scripta Mater.* 187 (2020) 445–452.
- [9] Q. Wang, J. Han, Y. Liu, Z. Zhang, C. Dong, P.K. Liaw, *Scripta Mater.* 190 (2021) 40–45.
- [10] W. Wu, S. Ni, Y. Liu, M. Song, *J. Mater. Res.* 31 (2016) 3815–3823.
- [11] O.N. Senkov, C. Woodward, D.B. Miracle, *Jom* 66 (2014) 2030–2042.
- [12] O.N. Senkov, C.F. Woodward, *Mater. Sci. Eng. A* 529 (2011) 311–320.
- [13] O.N. Senkov, J.M. Scott, S.V. Senkova, D.B. Miracle, C.F. Woodward, *J. Alloys Comp.* 509 (2011) 6043–6048.
- [14] N.D. Stepanov, N.Y. Yurchenko, S.V. Zharebtsov, M.A. Tikhonovsky, G.A. Salishchev, *Materials Letters* 211 (2018) 87–90.
- [15] G. Laplanche, P. Gadaud, L. Perrière, I. Guillot, J.P. Couzinié, *J. Alloys Comp.* 799 (2019) 538–545.
- [16] X. Yang, Y. Zhang, P.K. Liaw, *Procedia Eng* 36 (2012) 292–298.
- [17] O.N. Senkov, S.V. Senkova, C. Woodward, *Acta Materialia* 68 (2014) 214–228.
- [18] O.N. Senkov, G.B. Wilks, J.M. Scott, D.B. Miracle, *Intermetallics* 19 (2011) 698–706.
- [19] K. Biswas, J.-W. Yeh, P.P. Bhattacharjee, J.T.M. DeHosson, *Scripta Mater.* 188 (2020) 54–58.
- [20] I. Basu, J.T.M. De Hosson, *Scripta Mater.* 187 (2020) 148–156.
- [21] X. Liu, T. Ji, N. Li, Y. Liu, J. Yin, B. Su, J. Zhao, Y. Li, G. Mo, Z. Wu, *Materials & Design* 180 (2019) 107963.
- [22] R.R. Eleti, N. Stepanov, S. Zharebtsov, *Scripta Mater.* 188 (2020) 118–123.
- [23] D. Schliephake, A.E. Medvedev, M.K. Imran, S. Obert, D. Fabijanic, M. Heilmaier, A. Molotnikov, X. Wu, *Scripta Mater.* 173 (2019) 16–20.
- [24] J.W. Bae, J.G. Kim, J.M. Park, W. Woo, S. Harjo, H.S. Kim, *Scripta Mater.* 165 (2019) 60–63.
- [25] W.G. Nöhring, W.A. Curtin, *Scripta Mater.* 187 (2020) 210–215.
- [26] W.G. Nöhring, W.A. Curtin, *Acta Materialia* 128 (2017) 135–148.
- [27] C. Varvenne, A. Luque, W.A. Curtin, *Acta Materialia* 118 (2016) 164–176.
- [28] T. Mohri, Y. Chen, M. Kohyama, S. Ogata, A. Saengdeejeing, S.K. Bhattacharya, M. Wakeda, S. Shinzato, H. Kimizuka, *NPJ Comput. Mater.* 3 (2017) 10.
- [29] S. Yin, J. Ding, M. Asta, R.O. Ritchie, *NPJ Comput. Mater.* 6 (2020).
- [30] S.I. Rao, B. Akdim, E. Antillon, C. Woodward, T.A. Parthasarathy, O.N. Senkov, *Acta Materialia* 168 (2019) 222–236.